Environ. Sci. Technol. **2007**, *41,* 4317−4325

Emissions from Laboratory Combustion of Wildland Fuels: Emission Factors and Source Profiles

L.-W. ANTONY CHEN,*,† HANS MOOSMÜLLER,† W. PATRICK ARNOTT,†,§ JUDITH C. CHOW,† JOHN G. WATSON,† RONALD A. SUSOTT,‡ RONALD E. BABBITT,‡ CYLE E. WOLD,‡ EMILY N. LINCOLN,‡ AND WEI MIN HAO‡

Division of Atmospheric Sciences, Desert Research Institute, Nevada System of Higher Education, Reno, Nevada, and Fire Sciences Laboratory, Rocky Mountain Research Station, USDA Forest Service, Missoula, Montana

Combustion of wildland fuels represents a major source of particulate matter (PM) and light-absorbing elemental carbon (EC) on a national and global scale, but the emission factors and source profiles have not been well characterized with respect to different fuels and combustion phases. These uncertainties limit the accuracy of current emission inventories, smoke forecasts, and source apportionments. This study investigates the evolution of gaseous and particulate emission and combustion efficiency by burning wildland fuels in a laboratory combustion facility. Emission factors for carbon dioxide (CO_2), carbon monoxide (CO), total hydrocarbon (THC), nitrogen oxides (NO_x), PM, light extinction and absorption cross sections, and spectral scattering cross sections specific to flaming and smoldering phases are reported. Emission factors are generally reproducible within ±20% during the flaming phase, which, despite its short duration, dominates the carbon emission (mostly in the form of CO_2) and the production of light absorption and EC. Higher and more variable emission factors for CO, THC, and PM are found during the smoldering phase, especially for fuels containing substantial moisture. Organic carbon (OC) and EC mass account for a majority (i.e., >60%) of PM mass; other important elements include potassium, chlorine, and sulfur. Thermal analysis separates the EC into subfractions based on analysis temperature demonstrating that high-temperature EC (EC2; at 700 °C) varies from 1% to 70% of PM among biomass burns, compared to 75% in kerosene soot. Despite this, the conversion factor between EC and light absorption emissions is rather consistent across fuels and burns, ranging from 7.8 to 9.6 m^2/gEC. Findings from this study should be considered in the development of PM and EC emission inventories for visibility and radiative forcing assessments.

* Corresponding author e-mail: antony@dri.edu.
† Desert Research Institute.
‡ Rocky Mountain Research Station.
§ Current affiliation: Department of Physics, University of Nevada, Reno.

1. Introduction

Biomass burning in the U.S. accounts for more than one-third of primary $PM_{2.5}$ (particles with aerodynamic diameter <2.5 μm) emissions and is a major source of light-absorbing elemental carbon (EC), strongly affecting the atmospheric visibility and radiation budget (*1*, *2*). Today prescribed burning is commonly used as a land management tool to maintain forest health. The U.S. Environmental Protection Agency (*3*) lists prescribed burning as the third largest source of primary anthropogenic $PM_{2.5}$, behind only utility fuel and residential wood combustion. Major uncertainties in the assessment of prescribed burning impacts on air quality and climate have been attributed to inadequate emission factors, activity data, or both.

In natural and managed fires, a flame front passes rapidly through a fuel bed followed by sustained smoldering combustion, so emissions from both combustion phases coexist with their proportions quickly changing in space and time. While the most accurate emission factors would be those measured directly in the field during real fires, these by necessity represent a combination of vegetation and combustion phases and are influenced by the underlying soil moisture and other biomass (e.g., wood and grass duff). Because of the variability in actual burning conditions, extrapolating the measured emission factors from one study to other fires is uncertain. Laboratory-controlled fires are useful for isolating effects of individual parameters (e.g., fuel, moisture, combustion phase) on emission factors, but they do not fully anticipate or reproduce the complex real-world fires (e.g., *4*). It is, however, possible to estimate gaseous and PM emissions using field emission factors adjusted to reflect laboratory observations with modern emission models such as the Fire Emission Production Simulator (FEPS) (*5*).

This laboratory experiment was designed to monitor individual combustion events that proceed from ignition, through flaming and smoldering combustions, and ending with fire extinction. Measuring properties of burning emissions such as light scattering (σ_{scat}), light absorption (σ_{abs}), and particle mass concentration with second time resolution helps differentiate between flaming and smoldering emissions that are known to have distinct characteristics (*4*, *6*). The fuels tested were common wildland fuels mostly from mid-latitude biomes. This paper presents gas and particle emission factors and source profiles, and discusses their dependence on fuel and combustion phase.

2. Experimental Section

The experiment was conducted at the United States Forest Service (USFS) Fire Science Laboratory (FSL, Missoula, MT) from 11/19/03 to 11/26/03 (*7*, *8*). The combustion facilities at the FSL include a continuously weighed fuel bed under a 1.6 m diameter exhaust stack with a 3.6 m inverted-funnel opening extending from 2 m above the fuel bed through the ceiling (~22 m high). Goode et al. (*9*) show well- mixed and cooled plumes at the height of a sampling platform ~17 m above the bed. Sample air was drawn directly into instruments without additional dilution. This minimized the change in particle mass due to organics volatilization under different dilution ratios (e.g., *10*). Eight wildland fuels were examined: (1) ponderosa pine wood; (2) ponderosa pine needles; (3) white pine needles; (4) sagebrush; (5) excelsior; (6) Dambo grass; (7) Montana grass; and (8) tundra core (see detailed description in Table S1, Supporting Information). The first six fuels were "dry" from long-term indoor storage with a fuel moisture content of <10% of the dry mass and represent

10.1021/es062364i CCC: $37.00 © 2007 American Chemical Society
Published on Web 05/10/2007

wildland fuels during drought episodes. Montana grass and tundra core were relatively "wet" fuels (moisture content >10%) from Montana and Alaska, respectively. In addition, reference soot aerosol was generated by a kerosene lamp in one of the experiments.

About 250 g of fuel was used for each controlled fire (except tundra core which used 1250 g). Continuous gas and mass measurements of the effluent included: (1) CO_2 by infrared absorption (LI-840, Li-COR Environmental); (2) CO by infrared absorption (model 48C, Thermo Electron Corporation); (3) reactive nitrogen species (NO, NO_2, and NO_x) by chemiluminenscence (model 42C, Thermo Electron Corporation); (4) THC, including CH_4, by flame ionization detection (model 42C THC Analyzer, Thermo Electron Corporation); and (5) PM mass by inertial microbalance (TEOM, Series 1105, Rupprecht & Patashnick Compony). There was no size-selective inlet upstream of the TEOM, though it is believed that most of the PM mass is in the fine fraction (i.e., <2.5 μm). The TEOM mass was normalized to gravimetric analysis of simultaneous time-integrated Teflon-filter samples. Optical measurements included: (1) σ_{abs} at 532 and 1047 nm by photoacoustic detection (*11*); (2) σ_{ext} ($\sigma_{scat} + \sigma_{abs}$) at 532 nm by cavity ring-down/cavity enhanced detection (CRD/CED) (*12*); (3) σ_{scat} at 450, 550, and 700 nm by nephelometry (TSI 3563, TSI). The nephelometer reported total (σ_{scat}) and hemispheric back-scattering ($\beta\sigma_{scat}$), with their accuracy limited by the nephelometer truncation angle (i.e., 7°) (*13*). The nephelometer data are useful for calculating the spectral Ångström exponent (i.e., $\alpha_s = -\ln\lfloor\sigma_{scat,\lambda_1}/\sigma_{scat,\lambda_2}\rfloor/\ln[\lambda_1/\lambda_2]$), a semiquantitative indicator of particle size (*8*). The continuous instruments operated with a time resolution between 1 and 10 s. Precisions of PM mass and optical measurements have been discussed in Chen et al. (*8*).

Smoke PM was collected on Teflon-membrane and quartz-fiber filters for the quantification of mass (by gravimetry), multi-elements (by X-ray fluorescence (*14*)), and organic carbon (OC), EC and TC (OC + EC) concentrations. These samples represent time-integrated averages over individual burns, and contributions from different combustion phases were not separated. OC and EC were determined by both the IMPROVE and STN protocol (*15*) using a DRI model 2001 carbon analyzer. Source profiles based on elements and carbon fractions are presented and compared in this paper. Emission factors for organic species are presented elsewhere (*16*).

3. Results and Discussions

3.1 Definitions. The fundamental definition of fuel-based emission factor is the mass of a compound released per mass of fuel consumed (*17*). This is related to the amount of carbon in the fuel:

$$\mathrm{EF}_j = \frac{M_j}{M_{fuel}} = \frac{M_j}{C_{ash} + \sum_i C_i} x_{c,fuel} = \frac{M_j}{\sum_i C_i}\left(\frac{\sum_i C_i}{C_{ash} + \sum_i C_i}\right) x_{c,fuel} = \frac{M_j}{\sum_i C_i}\left(x_{c,fuel} - \frac{M_{ash}}{M_{fuel}} x_{c,ash}\right) \quad (1)$$

where EF_j = emission factor of species j; M_{fuel} = mass of the fuel burned; M_j = mass of the species j emitted; C_{ash} = carbon mass in ash; C_i = carbon mass in every combustion product i (CO_2, CO, etc., including species j); and $x_{c,fuel}$ and $x_{c,ash}$ = carbon mass fraction in fuel and ash, respectively.

For the fuels used here, $x_{c,fuel}$ is in the range of 45−50% (Table S1) except for kerosene fuel and tundra core. Since ash typically accounts for <5% of the fuel mass (*7*) and contains little carbon, the "ash term" in eq 1 can be ignored, making this equation for biomass burning identical to equations used for liquid fuel combustion (*18*).

To obtain time-resolved (dynamic) EFs, eq 1 is further modified for use with continuous measurements as

$$\mathrm{EF}_j = \frac{\overline{\Delta[M_j]}}{\sum_i x_{c,i}\overline{\Delta[M_i]}} x_{c,fuel} = \frac{\overline{\Delta[M_j]}}{\sum_i \overline{\Delta[C_i]}} x_{c,fuel} = \frac{\overline{\Delta[M_j]}}{\overline{[\mathrm{TotC}]}} x_{c,fuel} \quad (2)$$

where $\overline{\Delta[M_j]}$ is the average of excess mass concentration $\Delta[M_j]$ (i.e., above background level) of species j measured in the smoke for a sampling period. M_i includes M_{CO2}, M_{CO}, M_{THC}, and M_{PM} with $x_{c,i} \equiv M_i/C_i$. THC and PM consist of multiple species, but THC was already in units of ppm carbon. For $x_{c,PM}$, a nominal value of 0.75 is used, according to the carbon mass fraction of 0.5−1 in PM estimated from filter samples (see Section 3.3). TotC represents the total (gas + PM) carbon emission. The influence of $x_{c,PM}$ uncertainties on the EF calculation is negligible, i.e., < ±2% because the carbon emission is predominantly (>95%) in the form of CO_2 and CO.

Flaming and smoldering combustion are distinguished by their different combustion efficiencies (CE), defined as

$$\mathrm{CE} = \frac{x_{\mathrm{CO_2}}\overline{\Delta[M_{\mathrm{CO_2}}]}}{\sum_i x_{c,i}\overline{\Delta[M_i]}} = \frac{\overline{\Delta[C_{\mathrm{CO_2}}]}}{\overline{[\mathrm{TotC}]}} \quad (3)$$

the fraction of carbon emitted in the form of CO_2. Alternatively, one may use modified combustion efficiency (MCE) if only CO_2 and CO are measured (MCE = $\overline{\Delta[\mathrm{C_{CO_2}}]}/(\overline{\Delta[\mathrm{C_{CO_2}}]} + \overline{\Delta[\mathrm{C_{CO}}]})$). CE and MCE are usually close to 1 during the flaming phase due to near stochiometric combustion. When most volatiles have been expelled from the fuel surface, flaming ceases, and smoldering begins. Smoldering combustion is a lower-temperature oxidation process (<850 K) in the char layer that yields more CO and other incompletely oxidized pyrolysis products. Lee et al. (*4*) reports good correlations between CO_2 and many hydrocarbon species for smoldering emissions. Typical CE and MCE during smoldering phase are 0.7−0.9 (*6*, *19*, *20*).

Figure 1a and b exemplify the evolution of CE and MCE during a burn of white pine needles and sagebrush, respectively. CE and MCE exceed 0.98 for the first 1.5 min after ignition, and then rapidly decrease to <0.9 indicating the transition from flaming to smoldering. Despite a relatively short duration, the flaming phase dominates the carbon emission (TotC) and has a relatively high emission factor for σ_{abs} (note: σ_{abs} at 532 nm is caused by both PM and NO_2). As the smoldering combustion takes over, $\mathrm{EF_{PM}}$ and $\mathrm{EF}\sigma_{ext}$ increase, especially for the burning of white pine needles. In terms of TotC emission, smoldering combustion is less intense but can persist for a long time. In Figure 1b, the excess CO_2/CO concentrations remained at 2/0.2 ppm at the end of sampling when the PM level dropped below the TEOM detection limit. Smoke emissions during the smoldering phase exhibit a much higher single scattering albedo (ω_o, the fraction of σ_{ext} due to σ_{scat}) than that from the flaming phase. The other dry fuels show similar patterns (e.g., *8*). It is

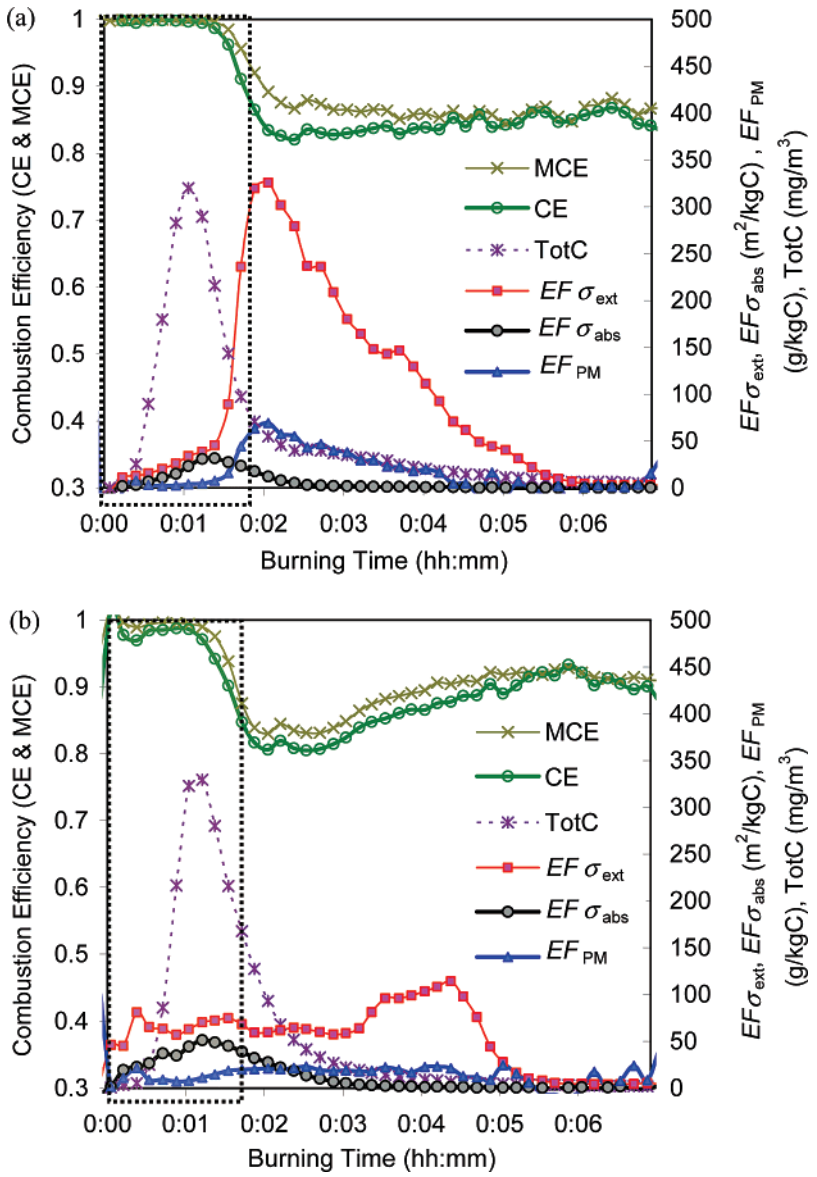

FIGURE 1. Time series of combustion efficiency (CE, MCE), total carbon (TotC) concentration, and instant (10 s) emission factors of extinction, absorption cross section (at 532 nm), and PM mass measured during combustion of (a) white pine needles and (b) sagebrush. Emission factors are normalized to TotC (i.e., in unit of g/kgC). The dashed box defines the flaming phase (see text for details).

desirable to separate emission factors for flaming and smoldering phases for emission inventory and smoke forecast applications. A perfect split, however, is unlikely because there is a transition period (0.9 < CE < 0.98; typically <1 min in this study) when flaming and smoldering combustion coexist. The lowest CE usually occurs at the end of this transition period. CE increases thereafter may be due to an increasing oxygen level as observed by Hays et al. (*21*), and this complicates the separation of flaming and smoldering phases based solely on a threshold CE or MCE (e.g., MCE = 0.9 as noted by Reid et al. (*6*) and references therein). Since CO is the most important marker for smoldering combustion, in this study the split is made so that the difference in $\overline{\Delta[M_{CO}]}/\overline{[TotC]}$ or average EF_{CO} between the flaming and smoldering phases is maximized. This occurs during the transition (e.g., Figure 1a and b) and is consistent with the visual observation of flaming and smoldering. The same criterion is applied to all the burns except for tundra core and kerosene combustion where only one phase could be identified.

3.2 Emission Factors. Average fuel-based emission factors for the flaming and smoldering phases are shown in Table 1. The consistency within 6−7 replicate burns for each fuel not only reflects the natural variability of the combustion process but also corroborates the estimate for $x_{c,PM}$ and the flaming/smoldering split point.

Most of the carbon emissions occur during the flaming phase, particularly for ponderosa pine wood (98 ±1%), excelsior (97 ± 1%), and Dambo grass (97 ± 2%). The dry fuels exhibit CE ≥ 0.97 and EFs reproducibility typically within ± 20% for CO, THC, NO, and PM, averaged over the flaming phase. However, large variations are observed among the different fuels. Sagebrush burning yields the highest EF_{CO} and EF_{THC}, more than twice those of white pine needles. EF_{PM} varies by a factor of 2.5. CE and MCE remain below 0.9 throughout the burning of wet tundra core (fuel moisture 113 ± 126%), and therefore no flaming phase is reported. Montana grass, a wet fuel containing 17.5% water (Table S1), shows a flaming phase but its fraction varies substantially between two replicate burns (C_F 60−90%). The smoke ω_o for this flaming phase is 0.95, much higher than those of dry fuels (i.e., 0.32−0.73), and the absorption is largely caused by NO_2 (Table 1). These could reflect a lower combustion temperature for wet fuels, or an unclear separation between

TABLE 1. Emission Factors (Average and 1σ) of Burning for the Flaming Phase, Smoldering Phase, and Overall Combustion[a]

Flaming Phase

	EF	PPWOOD	PPNEED	WPNEED	SAGE	EXCEL	DGRASS	MTGRASS[b]	KERO[c]
# of burn		7	7	6	6	6	6	2	1
C_F (%)		98% ± 1%	88% ± 5%	74% ± 1%	66% ± 5%	97% ± 1%	97% ± 2%	75% ± 15%	100%
CE		0.98 ± 0.00	0.97 ± 0.00	0.98 ± 0.00	0.96 ± 0.00	0.98 ± 0.00	0.98 ± 0.00	0.97−0.96	0.96
MCE		0.99 ± 0.00	0.98 ± 0.00	0.99 ± 0.00	0.98 ± 0.00	0.99 ± 0.00	0.98 ± 0.00	0.99−0.99	1.00
CO_2	g/kg fuel	1763.1 ± 2.4	1781.9 ± 8.7	1758.5 ± 4.7	1692.2 ± 7.3	1721.8 ± 2.3	1612.0 ± 5.0	1553.8 ± 11.6	3520.2
CO	g/kg fuel	15.1 ± 1.2	19.9 ± 4.3	11.2 ± 1.9	22.6 ± 4.1	16.1 ± 0.8	16.8 ± 1.0	11.7 ± 1.8	2.8
THC[d]	g/kg fuel	0.4 ± 0.2	3.3 ± 0.4	2.5 ± 0.6	6.3 ± 1.0	1.3 ± 0.3	2.1 ± 0.4	10.4 ± 1.6	n.d.
NO	g/kg fuel	0.5 ± 0.0	2.9 ± 0.2	2.5 ± 0.2	1.6 ± 0.5	0.8 ± 0.1	1.7 ± 0.1	4.3 ± 1.1	0.4
NO_2	g/kg fuel	0.3 ± 0.0	0.9 ± 0.3	0.6 ± 0.2	0.2 ± 0.1	0.1 ± 0.1	0.8 ± 0.1	4.8 ± 0.3	2.6
PM	g/kg fuel	3.2 ± 0.6	4.0 ± 0.5	5.0 ± 0.4	5.4 ± 0.6	3.4 ± 0.4	2.1 ± 1.0	4.5 ± 1.6	51.6
σ_{ext} (532 nm)	m^2/kg fuel	29.4 ± 2.9	28.6 ± 3.4	30.8 ± 1.8	31.2 ± 4.2	23.0 ± 3.2	12.1 ± 6.8	15.5 ± 7.5	578.7
σ_{abs} (532 nm)	m^2/kg fuel	20.1 ± 2.3	17.0 ± 2.0	9.8 ± 1.4	21.4 ± 3.6	14.5 ± 1.3	3.2 ± 0.6	0.7 ± 0.1	328.8
σ_{abs} (532 nm) by NO_2[e]	m^2/kg fuel	0.1 ± 0.0	0.1 ± 0.0	0.1 ± 0.0	0.0 ± 0.0	0.0 ± 0.0	0.1 ± 0.0	0.8 ± 0.1	0.4
σ_{abs} (1047 nm)	m^2/kg fuel	11.0 ± 1.3	9.3 ± 1.1	5.0 ± 0.8	10.5 ± 1.9	7.5 ± 0.7	1.5 ± 0.4		178.4
σ_{scat} (450/550/700 nm)[f]	m^2/kg fuel	7.8/5.6/3.6	10.0/7.0/4.3	19.1/15.0/10.6	11.0/7.3/4.3	11.1/7.8/4.8	9.2/6.6/4.3	16.0/13.0/9.9	131.2/95.4/62.7
$\beta\sigma_{scat}$ (450/550/700 nm)[f]	m^2/kg fuel	1.5/1.1/0.9	1.8/1.4/1.0	2.9/2.2/1.8	2.2/1.6/1.2	1.9/1.4/1.0	1.4/1.0/0.8	2.3/1.8/1.5	24.2/18.9/15.2

Smoldering Phase

	EF	PPWOOD	PPNEED	WPNEED	SAGE	EXCEL	DGRASS	MTGRASS[b]	TUNDRA[c]
# of burn		7	7	6	6	6	6	2	1
C_S (%)		2% ± 1%	12% ± 5%	26% ± 1%	34% ± 5%	3% ± 1%	3% ± 2%	25% ± 15%	100%
CE		0.88 ± 0.02	0.87 ± 0.04	0.80 ± 0.02	0.86 ± 0.02	0.82 ± 0.04	0.88 ± 0.03	0.50−0.78	0.76
MCE		0.89 ± 0.03	0.88 ± 0.04	0.85 ± 0.01	0.88 ± 0.02	0.86 ± 0.02	0.88 ± 0.02	0.82−0.94	0.87
CO_2	g/kg fuel	1573.8 ± 44.9	1596.9 ± 73.3	1445.0 ± 34.5	1506.4 ± 35.1	1436.0 ± 62.2	1447.3 ± 41.3	1031.7 ± 226.1	2784.0
CO	g/kg fuel	126.7 ± 30.0	134.9 ± 47.0	157.4 ± 7.2	131.5 ± 17.9	154.4 ± 14.5	121.7 ± 18.9	82.5 ± 31.8	270.9
THC[d]	g/kg fuel	1.7 ± 3.6	4.3 ± 1.7	14.5 ± 4.4	8.8 ± 2.0	9.9 ± 6.0	1.2 ± 4.6	125.3 ± 44.0	124.9
NO	g/kg fuel	1.3 ± 0.7	4.9 ± 1.9	2.5 ± 0.5	6.6 ± 0.5	5.0 ± 2.6	0.4 ± 0.5	4.8 ± 0.5	2.0
NO_2	g/kg fuel	1.1 ± 0.3	2.1 ± 1.1	0.9 ± 0.2	0.7 ± 0.2	2.2 ± 1.4	0.4 ± 0.3	10.2 ± 1.9	1.1
PM	g/kg fuel	7.0 ± 11.5	4.6 ± 2.0	23.4 ± 6.8	8.2 ± 2.2	19.7 ± 11.7	3.0 ± 6.2	39.1 ± 20.1	41.3
σ_{ext} (532 nm)	m^2/kg fuel	6.7 ± 0.9	13.5 ± 6.9	114.4 ± 28.2	27.8 ± 13.6	76.6 ± 49.4	4.5 ± 6.1	194.7 ± 115.4	668.4
σ_{abs} (532 nm)	m^2/kg fuel	2.6 ± 1.5	4.6 ± 3.9	1.1 ± 0.2	9.8 ± 2.1	9.3 ± 4.0	0.3 ± 0.3	1.8 ± 0.7	3.4
σ_{abs} (532 nm) by NO_2[e]	m^2/kg fuel	0.2 ± 0.1	0.3 ± 0.2	0.2 ± 0.0	0.1 ± 0.0	0.4 ± 0.2	0.1 ± 0.0	1.7 ± 0.3	0.2
σ_{abs} (1047 nm)	m^2/kg fuel	0.8 ± 0.8	0.5 ± 0.5	0.3 ± 0.1	4.5 ± 1.1	3.2 ± 1.7	0.0 ± 0.3		
σ_{scat} (450/550/700 nm)[f]	m^2/kg fuel	5.2/3.1/1.8	8.6/5.6/3.4	100.9/85.0/66.3	26.0/17.0/9.7	73.4/54.8/36.8	5.2/3.3/2.2	153.5/125.1/95.4	441.4/360.8/276.9
$\beta\sigma_{scat}$ (450/550/700 nm)[f]	m2/kg fuel	1.0/0.7/0.4	1.4/1.0/0.8	12.4/10.2/9.2	4.0/3.0/2.2	9.8/7.4/6.2	0.7/0.4/0.3	20.2/16.3/14.6	51.9/42.9/37.9

	EF	PPWOOD	PPNEED	Overall WPNEED	SAGE	EXCEL	DGRASS	MTGRASS[b]
# of burn		7	7	6	6	6	6	2
CE		0.98 ± 0.00	0.96 ± 0.00	0.93 ± 0.01	0.93 ± 0.01	0.97 ± 0.00	0.97 ± 0.01	0.91−0.89
MCE		0.99 ± 0.00	0.97 ± 0.00	0.96 ± 0.00	0.95 ± 0.01	0.98 ± 0.00	0.98 ± 0.00	0.98−0.97
CO_2	g/kg fuel	1759.8 ± 2.1	1762.5 ± 5.5	1677.4 ± 9.1	1628.2 ± 14.7	1712.2 ± 4.6	1606.6 ± 10.2	1456.4 ± 15.0
CO	g/kg fuel	17.0 ± 0.5	32.0 ± 3.3	49.0 ± 2.0	60.0 ± 6.5	20.7 ± 1.5	20.1 ± 4.0	24.8 ± 1.5
THC[d]	g/kg fuel	0.4 ± 0.2	3.5 ± 0.5	5.6 ± 1.5	7.2 ± 1.2	1.6 ± 0.4	2.1 ± 0.5	32.6 ± 5.4
NO	g/kg fuel	0.5 ± 0.0	3.1 ± 0.2	2.5 ± 0.1	3.3 ± 0.2	0.9 ± 0.0	1.7 ± 0.1	4.5 ± 0.9
NO_2	g/kg fuel	0.3 ± 0.0	1.0 ± 0.3	0.7 ± 0.2	0.3 ± 0.1	0.2 ± 0.1	0.8 ± 0.1	6.5 ± 1.1
PM	g/kg fuel	3.3 ± 0.8	4.0 ± 0.6	9.8 ± 1.8	6.4 ± 0.9	3.9 ± 0.6	2.2 ± 1.1	10.3 ± 0.9
σ_{ext} (532 nm)	m^2/kg fuel	29.0 ± 2.8	26.7 ± 2.5	52.3 ± 6.9	30.2 ± 5.1	24.9 ± 4.7	11.9 ± 6.6	43.7 ± 7.0
σ_{abs} (532 nm)	m^2/kg fuel	19.8 ± 2.2	15.5 ± 1.2	7.6 ± 1.0	17.4 ± 2.3	14.3 ± 1.3	3.2 ± 0.7	0.9 ± 0.0
σ_{abs} (532 nm) by NO_2[e]	m^2/kg fuel	0.1 ± 0.0	0.2 ± 0.0	0.1 ± 0.0	0.1 ± 0.0	0.0 ± 0.0	0.1 ± 0.0	1.0 ± 0.2
σ_{abs} (1047 nm)	m^2/kg fuel	10.8 ± 1.3	8.2 ± 0.7	3.8 ± 0.6	8.4 ± 1.3	7.4 ± 0.7	1.5 ± 0.4	
σ_{scat} (450/550/700 nm)[f]	m^2/kg fuel	7.7/5.5/3.5	9.9/6.9/4.2	40.2/33.1/25.0	16.3/10.7/6.3	13.4/9.5/6.0	9.1/6.5/4.2	38.5/30.9/23.4
$\beta\sigma_{scat}$ (450/550/700 nm)[f]	m^2/kg fuel	1.5/1.1/0.8	1.8/1.3/1.0	5.4/4.3/3.7	2.9/2.1/1.5	2.2/1.6/1.2	1.4/1.0/0.8	5.4/4.2/3.6

[a] C_F and C_S represent the percentage of carbon emission measured from the flaming phase and smoldering phase, respectively. PPWOOD: ponderosa pine wood; PPNEED: ponderosa pine needles; WPNEED: white pine needles; SAGE: sagebrush; EXCEL: shredded aspen wood product; DGRASS: Dambo grass; MTGRASS: Montana grass; TUNDRA: tundra core; KERO: kerosene flame soot. [b] Uncertainties for MTGRASS are half the difference of two replicate burns. [c] Emission factors are presented in g/kgC (per kg carbon) in fuel since the carbon mass fraction in fuel was not determined. [d] EF_{THC} is reported as gCH_4/kg fuel, i.e., an average molecular weight of 16 per carbon atom. [e] σ_{abs} by NO_2 is calculated using an absorption efficiency of 0.306 Mm^{-1}/ppb NO_2 at 532 nm. [f] Nephelometer data are without any truncation correction.

the flaming and smoldering phases. The kerosene flame emits little CO and THC but an extremely high quantity of particles with an overall ω_o of 0.43.

EFs for the smoldering phase are more variable for several reasons. In the combustion of ponderosa pine wood, excelsior, and Dambo grass, only 2−3% of carbon emissions came from the smoldering phase, resulting in very low gas and particle concentrations with large relative measurement uncertainties. In addition, smoldering combustion is a slow oxidation process for which emission factors may be more sensitive to the inhomogeneity in fuel, char, and combustion temperature. EF_{CO} increased by nearly an order of magnitude when entering the smoldering phase for most of the burns. Particle emissions did not increase as much, but the particles appear to be less light-absorbing and larger in size (*7*, *8*). Tundra core EF values for THC, PM, and σ_{ext} are among the largest of all the fuels tested. Smoldering CE and MCE are between 0.8 and 0.9 for all dry fuels and lower values (CE < 0.8) are found for wet fuels.

Although smoldering combustion consumes only a minor fraction of fuel mass, it dominates CO, THC, and PM emissions during the white pine needles and Montana grass burns (Figure S1, Supporting Information). For sagebrush, 75% of CO and nearly half of THC and PM are emitted during the smoldering phase. NO and NO_2 emissions are suggested to occur mostly during flaming combustion (e.g., *22*); sagebrush burning represents the only exception observed in this study. While σ_{abs} is another main product of the flaming phase, the smoldering phase can contribute substantial σ_{ext} and σ_{scat}. Fuels containing plant leaves, such as sagebrush, grasses, and pine needles, often have a higher nitrogen content (Table S1). Overall NO_x emissions are consistent with the nitrogen content in the fuel.

Emission factors reviewed by Andreae and Merlet (*17*) representing integrated field burning generally fall within the range of EFs determined for the flaming and smoldering phases for similar fuels in this study. For example, EF_{CO} for Andreae and Merlet's savanna grass burning is 65 ± 20 g/kg fuel, compared with 16.8 ± 1.0 g/kg fuel (flaming) and 121.7 ± 18.9 g/kg fuel (smoldering) from Dambo grass burning; $EF_{PM(fine)}$ for Andreae and Merlet's extratropical forest fire is 13 ± 7 g/kg fuel, compared with 5.0 ± 0.4 g/kg fuel (flaming) and 23.4 ± 6.8 g/kg fuel (smoldering) from white pine needle burning. Lee et al. (*4*) report EF_{CO} of ∼31 and ∼75 g/kg fuel (assuming $x_{c,fuel} = 0.5$) for flaming and smoldering combustion of a pine-dominated forest in the southeastern U.S., both of which are between the flaming EF_{CO} (11.2−19.9 g/kg fuel) and smoldering EF_{CO} (126.7−157.4 g/kg fuel) determined for ponderosa pine wood/needles and white pine needles in this study. Flaming and smoldering combustion is less separated during the measurements of real-world fires. Moreover, due to the influence of underlying soil and biomass, the partition of flaming and smoldering contribution (e.g., C_F and C_S in Table 1) may differ between real and simulated fires. This partly explains why the overall (entire-burn) EFs in Table 1, which are dominated by the flaming-phase EFs, differ from those given by Lee et al. and Andreae and Merlet. If CO_2 and CO are measured, however, MCE should provide an estimate for the flaming and smoldering partition in any particular burn, and that could be used to construct the total emission with phase-specific emission factors.

3.3 PM Source Profiles. Mass fractions of species measured in PM are shown in Table 2. These are composite chemical profiles resulting from the average of mass fractions from replicate samples burning the same fuel, as the approach described by Chow et al. (*23*). Carbon is the dominant component in PM, though the TC content in PM varies from 63.7% (sagebrush) to nearly 100% (ponderosa pine wood, Dambo grass, and tundra core). The carbon content was

TABLE 2. Mass Percentage (Average and 1σ) of Elements and Carbon Fractions in PM Emitted from Burning of Wildland Fuels and Kerosene. Carbon Fractions Are Determined by the IMPROVE and STN Thermal Protocols.

species	ponderosa pine wood	ponderosa pine needles	white pine needles	sagebrush	excelsior	Dambo grass	Montana grass	tundra core	kerosene soot
OC[a] (IMPROVE)	15.64 ± 7.52	31.42 ± 4.09	51.45 ± 6.22	28.01 ± 7.50	29.44 ± 8.00	62.6 ± 8.05	69.60 ± 14.07	93.5 ± 18.67	39.75 ± 11.91
EC (IMPROVE)	80.41 ± 4.85	57.27 ± 3.87	17.48 ± 3.94	35.68 ± 3.45	51.21 ± 3.19	35.5 ± 13.04	5.62 ± 7.15	2.64 ± 1.65	79.50 ± 12.05
TC (IMPROVE)	96.05 ± 8.88	88.70 ± 6.98	68.93 ± 4.79	63.69 ± 4.61	80.65 ± 10.45	98.21 ± 9.30	75.22 ± 21.22	96.2 ± 11.60	119.25 ± 16.80
OC1 (IMPROVE)	1.72 ± 2.29	2.29 ± 2.28	8.47 ± 3.99	2.14 ± 0.93	1.52 ± 1.64	3.09 ± 1.83	0.04 ± 3.93	11.74 ± 1.64	6.77 ± 8.91
OC2 (IMPROVE)	5.51 ± 3.58	7.85 ± 2.01	14.05 ± 1.40	6.88 ± 1.58	7.05 ± 2.12	15.11 ± 5.00	16.28 ± 4.35	30.09 ± 5.13	16.04 ± 9.28
OC3 (IMPROVE)	6.60 ± 1.85	13.37 ± 2.46	19.32 ± 2.73	12.46 ± 5.88	13.82 ± 2.95	24.86 ± 3.73	33.04 ± 9.24	31.92 ± 6.24	13.90 ± 9.29
OC4 (IMPROVE)	1.81 ± 1.63	7.01 ± 2.03	8.12 ± 1.71	5.96 ± 1.44	6.63 ± 1.43	13.91 ± 2.37	12.38 ± 4.35	12.36 ± 3.06	3.03 ± 8.94
OP (IMPROVE)	0.00 ± 1.61	0.90 ± 1.90	1.50 ± 2.12	0.56 ± 0.92	0.43 ± 1.23	5.72 ± 2.47	7.86 ± 5.03	7.47 ± 4.52	0.00 ± 8.91
EC1 (IMPROVE)	10.33 ± 1.97	55.92 ± 6.35	15.57 ± 3.65	35.14 ± 4.18	47.09 ± 5.17	16.66 ± 10.38	5.38 ± 3.96	5.97 ± 1.83	3.21 ± 8.92
EC2 (IMPROVE)	70.01 ± 5.35	2.26 ± 1.90	3.10 ± 1.40	1.10 ± 0.92	4.37 ± 1.25	23.50 ± 6.67	7.50 ± 3.94	3.81 ± 1.65	75.40 ± 9.97
EC3 (IMPROVE)	0.06 ± 1.61	0.00 ± 1.89	0.30 ± 0.63	0.00 ± 0.91	0.19 ± 1.20	1.08 ± 2.01	0.59 ± 3.94	0.33 ± 1.65	0.89 ± 8.94
OC (STN)	41.65 ± 9.37	44.19 ± 10.08	63.98 ± 13.58	41.06 ± 8.87	47.55 ± 10.33	88.24 ± 19.00	76.35 ± 12.74	98.2 ± 20.84	60.96 ± 15.67
EC (STN)	79.83 ± 6.50	44.64 ± 4.92	7.23 ± 1.27	22.39 ± 2.42	35.38 ± 3.46	6.79 ± 3.65	-0.03 ± 3.93	0.46 ± 1.63	65.95 ± 10.06
Al	0.287 ± 0.119	0.505 ± 0.162	0.297 ± 0.103	0.498 ± 0.077	0.221 ± 0.111	0.532 ± 0.379	0.259 ± 0.233	0.148 ± 0.097	0.683 ± 0.529
Si	0.371 ± 0.056	0.638 ± 0.211	0.611 ± 0.174	0.270 ± 0.138	0.276 ± 0.052	0.698 ± 0.549	0.424 ± 0.115	0.279 ± 0.047	1.065 ± 0.249
P	0.063 ± 0.041	0.115 ± 0.056	0.013 ± 0.007	0.188 ± 0.075	0.094 ± 0.024	0.104 ± 0.066	0.061 ± 0.067	0.020 ± 0.009	0.143 ± 0.049
S	0.540 ± 0.136	1.292 ± 0.211	0.342 ± 0.029	2.929 ± 0.153	1.005 ± 0.127	1.248 ± 0.689	0.183 ± 0.047	0.163 ± 0.003	1.113 ± 0.021
Cl	0.635 ± 0.136	5.605 ± 2.502	0.701 ± 0.227	9.643 ± 0.447	0.331 ± 0.161	0.321 ± 0.080	0.078 ± 0.042	0.142 ± 0.007	0.064 ± 0.037
K	2.108 ± 0.034	7.816 ± 2.119	1.063 ± 0.169	23.709 ± 0.050	5.757 ± 0.099	2.900 ± 2.598	0.486 ± 0.062	0.407 ± 0.001	0.842 ± 0.002
Ca	0.503 ± 0.042	0.458 ± 0.095	0.352 ± 0.063	0.192 ± 0.102	1.112 ± 0.011	0.295 ± 0.180	0.011 ± 0.019	0.218 ± 0.008	0.207 ± 0.043
Ti	0.017 ± 0.024	0.002 ± 0.006	0.035 ± 0.021	0.002 ± 0.004	0.000 ± 0.005	0.000 ± 0.013	0.000 ± 0.011	0.003 ± 0.005	0.000 ± 0.025
Mn	0.013 ± 0.025	0.058 ± 0.027	0.029 ± 0.011	0.008 ± 0.016	0.019 ± 0.027	0.023 ± 0.058	0.045 ± 0.050	0.029 ± 0.021	0.000 ± 0.113
Fe	0.152 ± 0.053	0.132 ± 0.080	0.243 ± 0.024	0.090 ± 0.044	0.093 ± 0.042	0.234 ± 0.331	0.165 ± 0.074	0.137 ± 0.031	0.366 ± 0.170
Ni	0.050 ± 0.038	0.046 ± 0.036	0.025 ± 0.006	0.024 ± 0.012	0.022 ± 0.017	0.069 ± 0.052	0.083 ± 0.087	0.017 ± 0.006	0.048 ± 0.030
Cu	0.241 ± 0.162	0.209 ± 0.124	0.163 ± 0.008	0.117 ± 0.009	0.164 ± 0.051	0.259 ± 0.103	0.548 ± 0.451	0.084 ± 0.005	0.620 ± 0.025
Zn	0.214 ± 0.092	0.165 ± 0.033	0.083 ± 0.018	0.140 ± 0.014	0.202 ± 0.010	0.146 ± 0.070	0.309 ± 0.245	0.044 ± 0.006	0.286 ± 0.033
Se	0.000 ± 0.005	0.000 ± 0.005	0.000 ± 0.002	0.010 ± 0.014	0.000 ± 0.005	0.000 ± 0.011	0.000 ± 0.010	0.000 ± 0.004	0.000 ± 0.022
Br	0.000 ± 0.006	0.007 ± 0.010	0.002 ± 0.003	0.008 ± 0.004	0.011 ± 0.015	0.006 ± 0.013	0.014 ± 0.020	0.000 ± 0.005	0.095 ± 0.025
Pb	0.015 ± 0.021	0.000 ± 0.020	0.005 ± 0.008	0.008 ± 0.012	0.014 ± 0.017	0.006 ± 0.042	0.000 ± 0.036	0.012 ± 0.015	0.000 ± 0.081
SUM[b]	101.26 ± 8.89	105.74 ± 7.72	72.89 ± 4.81	101.52 ± 4.64	89.97 ± 10.46	105.05 ± 9.71	77.88 ± 21.23	97.92 ± 11.60	124.78 ± 16.81
OM/OC[c] (IMPROVE)	0.93 ± 0.55	1.07 ± 0.19	1.51 ± 0.20	1.78 ± 0.49	1.41 ± 0.40	0.88 ± 0.24	1.32 ± 0.29	1.01 ± 0.20	0.27 ± 0.32

[a] OC and organic fractions may contain organic vapors adsorbed on the quartz-fiber filter. [b] Sum of measured species includes TC (IMPROVE) and all elemental species. [c] [OM] = [PM] − 4.125[S] − 2.2[Al] − 2.49[Si] − 1.63[Ca] − 2.42 [Fe] − 1.94[Ti] − [EC] (IMPROVE).

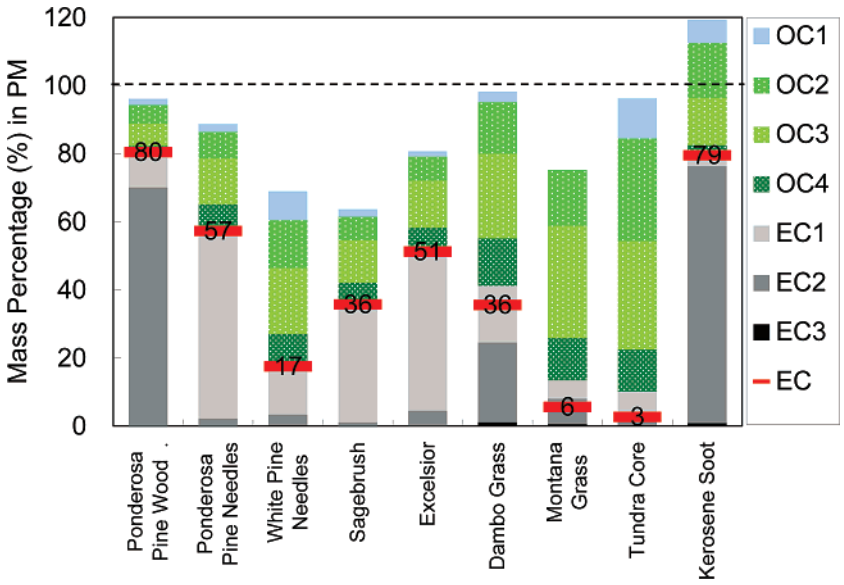

FIGURE 2. Mass percentage of thermally resolved carbon fractions in PM. The numbers indicate the mass percentage of EC. OP is the difference between EC1 + EC2 + EC3 and EC (i.e., OP is the gray area above the red bar).

determined from quartz-fiber filters in which adsorbed organic vapors are measured as OC (*24*). This may have inflated the particulate OC fraction and explains why TC exceeds 100% PM mass in kerosene soot (Table 2, the PM mass is determined gravimetrically using Teflon-membrane filters that do not adsorb organic vapors). EC is not strongly influenced by vapor adsorption. The actual carbon content in PM is likely between 50% and 100%. A wide range of the organic mass (OM)/OC ratio estimated from mass closure (Table 2) reflects uncertainties from the sampling artifact, OC/EC split, and potential unaccounted species.

Elemental potassium (K), chlorine (Cl), and sulfur (S) make up most of the remaining PM mass. The mass percentages of K and Cl can be as high as 23.7% and 9.6%, respectively, in sagebrush, but they are particularly low (<1%) in the smoke of the two wet fuels (Montana grass and tundra core). In the ponderosa pine wood smoke, the PM contains 2.1%, 0.64%, 0.54%, and 0.21% of K, Cl, S, and Zn, respectively, consistent with other measurements for ponderosa pine slash burning (*25*). The copper (Cu) content, however, is almost 2 orders of magnitude higher (0.24% in this study versus 0.0038% in Turn et al. (*25*)), possibly due to contamination from copper sampling lines. The sum of species appears to explain all the PM mass except for white pine needles and Montana grass, where the OC fraction is relatively high. Oxygen (O), nitrogen, and hydrogen associated with OC, S, and crustal elements are not included in the summed mass.

EC abundances from the IMPROVE protocol are higher than those from the STN protocol for all cases in Table 2. This difference is mostly a result of different charring corrections (i.e., reflectance versus transmittance), as discussed in Chow et al. (*15*) and Chen et al. (*26*). The IMPROVE protocol further segregates the PM carbon into eight operationally defined fractions with OC1, OC2, OC3, and OC4 evolved at 120, 250, 450, and 550 °C, respectively, in a pure helium (He) atmosphere and EC1, EC2, and EC3 evolved at 550, 700, and 800 °C in a 2% O_2/98% He atmosphere. OP represents the pyrolyzed carbon determined from the change in filter reflectance (*26*). These OC and EC subfractions are reported by the nationwide IMPROVE monitoring network and have been found useful for PM source apportionment (*27*–*29*).

As shown in Figure 2, the wood smoke is relatively rich in EC, while needles, grass, and tundra core combustion yield higher OC fractions. Most of the EC should originate from the flaming combustion. The EC subfractions vary dramatically between different fuels. Ponderosa pine wood burning resembles the kerosene flame, emitting EC that is dominated (88−95%) by the high-temperature EC2 (i.e., 700 °C). Dambo grass also produces a higher EC2 fraction (~66% of EC), but EC1 is more abundant in other burns (Figure 2). EC2 is often used as a marker for diesel soot (e.g., *28*, *30*). Due to lower combustion temperatures, gasoline vehicle and wood combustion are not expected to produce abundant EC2. This experiment shows otherwise. For OC subfractions, the majority is high-temperature OC3 and OC4 in all the samples tested (except for kerosene soot), in contrast to gasoline and diesel exhausts where OC1 and OC2 are more abundant (*30*, *31*). OC3 and OC4 likely represent polar and/or high-molecular-weight organic compounds that are less volatile. The amount of OP also tends to increase with the OC3 and OC4 content.

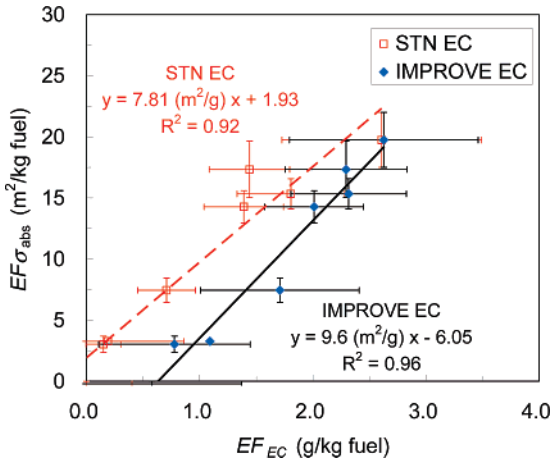

FIGURE 3. Relation between light absorption (at 532 nm and corrected for NO_2 light absorption) emission factors and EC emission factors measured by the IMPROVE and STN carbon analysis protocols. The scatter plot includes all fuels in this study except kerosene. Unweighted linear regression is used to calculate the slope and intercept.

3.4 Relations of EC with σ_{abs} and CO. The mass specific absorption efficiency of kerosene soot was determined to be

6.3 m^2/gPM at 532 nm (*8*). Thermal analysis found its EC mass fraction at 79% and 66% of PM by the IMPROVE and STN protocols, respectively. This translates to an EC mass absorption efficiency of 8.0 m^2/g (IMPROVE) and 9.6 m^2/g (STN). The conversion factor between EF_{EC} and $EF\sigma_{abs}$ (532 nm) emitted from biomass combustion in this study is in the same range, i.e., 9.6 ± 0.8 m^2/g by the IMPROVE protocol to 7.8 ± 0.9 m^2/g by the STN protocol based on regression slopes (Figure 3). These values might have been influenced by a large regression intercept for both IMPROVE and STN, which is consistent with biases in optical charring correction when EC concentrations are low (e.g., *26*). We can also calculate the conversion factor for individual burns using the $EF\sigma_{abs}/EF_{EC}$ ratio. The highest two EC emission factors (IMPROVE EC) are 2.6 ± 0.8 g/kg fuel for ponderosa pine wood burning and 2.3 ± 0.5 g/kg fuel for ponderosa pine needle burning. Although the thermal properties of EC differ (i.e., abundant EC2 in ponderosa pine wood versus EC1 in ponderosa pine needles), the conversion factors are similar (7.5 ± 0.9 m^2/g EC versus 6.6 ± 0.5 m^2/g EC at 532 nm).

CO has been used to estimate the EC emissions on regional and global scales (e.g., *32*, *33*) because both CO and EC result from incomplete combustions and CO emission inventories are relatively well developed. This study suggests that EC and CO are predominately emitted from flaming and smoldering combustion, respectively. This calls into question the use of CO emissions as surrogate for EC emissions from biomass burning since their relationship depends on the contribution from each combustion phase. Information on fuel and combustion conditions within the geographical domain of interest will be needed to refine the current approach. The IMPROVE EC/CO ratios determined in this study are as follows: ponderosa pine wood (0.15 g/g), ponderosa pine needles (0.072 g/g), white pine needles (0.035 g/g), Dambo grass (0.039 g/g), sagebrush (0.038 g/g), excelsior (0.097 g/g), Montana grass (0.023 g/g), and tundra core (0.004 g/g). These values are higher than the $\Delta[M_{EC}]/\Delta[M_{CO}]$ ratio measured in ambient air dominated by on-road motor vehicle emissions in North America (0.003−0.007 g/g (*32*)) but closer to measurements in South Asia that represent a mixture of biomass and fossil fuel combustions (0.013−0.027 g/g (*33*)).

Acknowledgments

This work was supported in part by the Joint Venture Agreement 03-JV-11222049-102 between the USFS, Rocky Mountain Research Station, Research Work Unit Number 4404 and DRI. Additional support was provided by California Air Resource Board Grant 04-307, USEPA Grant RD-83108601-0, and Joint Fire Science Project through NPS Task J8R07060005. Development of the DRI photoacoustic and cavity ringdown/cavity enhanced detection instruments was supported under NSF grants ATM-0340423 and ATM-9871192. We acknowledge S. Baker, V. Kovalev, S. Leininger, J. Newton, L. Rinehart, and C. Ryan for their efforts at the USFS Fire Science Laboratory.

Supporting Information Available

Specifications of wildland fuels used for the 2003 pilot study and fractional contributions of flaming phase and smoldering phase to the gaseous and particulate emissions. This material is available free of charge via the Internet at http://pubs.acs.org.

Literature Cited

(1) Watson, J. G. Visibility: Science and regulation. *J. Air Waste Manage. Assoc.* **2002**, *52*, 628−713.

(2) Kasischke, E. S.; Penner, J. E. Improving global estimates of atmospheric emissions from biomass burning. *J. Geophys. Res.* **2004**, *109*, D14S01, doi: 10.1029/2004JD004972.

(3) USEPA. *Air Quality Criteria for Particulate Matter*; EPA/600/P-99/002aF; EPA/600/P-99/002bF; U.S. EPA: Washington, DC, 2004.

(4) Lee, S.; Baumann, K.; Schauer, J. J.; Sheesley, R. J.; Naeher, L. P.; Meinardi, S.; Blake, D. R.; Edgerton, E. S.; Russell, A. G.; Clements, M. Gaseous and particulate emissions from prescribed burning in Georgia. *Environ. Sci. Technol.* **2005**, *39*, 9049−9056.

(5) Anderson, G.; Sandberg, D.; Norheim, R. *Fire Emission Production Simulator (FEPS) User's Guide*; U.S. Forest Service: Washington, DC, 2004.

(6) Reid, J. S.; Koppmann, R.; Eck, T. F.; Eleuterio, D. P. A review of biomass burning emissions part II: intensive physical properties of biomass burning particles. *Atmos. Chem. Phys.* **2005**, *5*, 799−825.

(7) Chakrabarty, R. K.; Moosmüller, H.; Garro, M. A.; Arnott, W. P.; Walker, J.; Susott, R. A.; Babbitt, R. E.; Wold, C. E.; Lincoln, E. N.; Hao, W. M. Emissions from the laboratory combustion of wildland fuels: Particle morphology and size. *J. Geophys. Res.* **2006**, *111*, D07204, doi: 10.1029/2005JD006659.

(8) Chen, L.-W. A.; Moosmüller, H.; Arnott, W. P.; Chow, J. C.; Watson, J. G.; Susott, R. A.; Babbitt, R. E.; Wold, C.; Lincoln, E.; Hao, W. M. Particle emissions from laboratory combustion of wildland fuels: In situ optical and mass measurements. *Geophys. Res. Lett.* **2006**, *33*, 1−4, doi: 10.1029/2005GL024838.

(9) Goode, J. G.; Yokelson, R. J.; Susott, R. A.; Ward, D. E. Trace gas emissions from laboratory biomass fires measured by Fourier transform infrared spectroscopy: Fires in grass and surface fuels. *J. Geophys. Res.* **1999**, *104*, 21237−21245.

(10) Lipsky, E. M.; Robinson, A. L. Effects of dilution on fine particle mass and partitioning of semivolatile organics in diesel exhaust and wood smoke. *Environ. Sci. Technol.* **2006**, *40*, 155−162.

(11) Arnott, W. P.; Moosmüller, H.; Walker, J. W. Nitrogen dioxide and kerosene-flame soot calibration of photoacoustic instruments for measurement of light absorption by aerosols. *Rev. Sci. Instrum.* **2000**, *71*, 4545−4552.

(12) Moosmüller, H.; Varma, R.; Arnott, W. P. Cavity ring-down and cavity-enhanced detection techniques for the measurement of aerosol extinction. *Aerosol Sci. Technol.* **2005**, *39*, 30−39.

(13) Anderson, T. L.; Covert, D. S.; Marshall, S. F.; Laucks, M. L.; Charlson, R. J.; Waggoner, A. P.; Ogren, J. A.; Caldow, R.; Holm, R. L.; Quant, F. R.; Sem, G. J.; Wiedensohler, A.; Ahlquist, N. C.; Bates, T. S. Performance characteristics of a high-sensitivity, three-wavelength, total scatter/backscatter nephelometer. *J. Atmos. Ocean. Technol.* **1996**, *13*, 967−986.

(14) Watson, J. G.; Chow, J. C.; .Frazier, C. A. X-ray fluorescence analysis of ambient air samples. In *Elemental Analysis of Airborne Particles, Vol. 1*; Landsberger, S., Creatchman, M., Eds.; Gordon and Breach Science: Amsterdam, 1999; Ch. 2.

(15) Chow, J. C.; Watson, J. G.; Chen, L.-W. A.; Arnott, W. P.; Moosmüller, H.; Fung, K. K. Equivalence of elemental carbon by Thermal/Optical Reflectance and Transmittance with different temperature protocols. *Environ. Sci. Technol.* **2004**, *38*, 4414−4422.

(16) Mazzoleni, L. R.; Zielinska, B.; Moosmüller, H. Emissions of levoglucosan, methoxy phenols, and organic acids from prescribed burns, wildland fuels, and residential wood combustion. *Environ. Sci. Technol.* **2007**, *41* (7), 2115−2122.

(17) Andreae, M. O.; Merlet, P. Emission of trace gases and aerosols from biomass burning. *Global Biogeochem. Cycles* **2001**, *15*, 955−966.

(18) Moosmüller, H.; Mazzoleni, C.; Barber, P. W.; Kuhns, H. D.; Keislar, R. E.; Watson, J. G. On-road measurement of automotive particle emissions by ultraviolet lidar and transmissometer: Instrument. *Environ. Sci. Technol.* **2003**, *37*, 4971−4978.

(19) Yokelson, R. J.; Susott, R.; Ward, D. E.; Reardon, J.; Griffith, D. W. T. Emissions from smoldering combustion of biomass measured by open- path Fourier transform infrared spectroscopy. *J. Geophys. Res.* **1997**, *102*, 18865−18877.

(20) Hao, W.-M.; Ward, D. E. Methane production from global biomass burning. *J. Geophys. Res.* **1993**, *98*, 20657−20661.

(21) Hays, M. D.; Fine, P. M.; Geron, C. D.; Kleeman, M. J.; Gullett, B. K. Open burning of agricultural biomass: Physical and chemical properties of particle-phase emissions. *Atmos. Environ.* **2005**, *39*, 6747−6764.

(22) Ferek, R. J.; Reid, J. S.; Hobbs, P. V.; Blake, D. R.; Liousse, C. Emission factors of hydrocarbons, halocarbons, trace gases, and particles from biomass burning in Brazil. *J. Geophys. Res.* **1998**, *103*, 32107−32118.

(23) Chow, J. C.; Watson, J. G.; Ashbaugh, L. L.; Magliano, K. L. Similarities and differences in PM_{10} chemical source profiles for geological dust from the San Joaquin Valley, California.

Atmos. Environ. **2003**, *37*, 1317−1340, doi: 10.1016/S1352−2310-(02)01021-X.
(24) Turpin, B. J.; Huntzicker, J. J.; Hering, S. V. Investigation of organic aerosol sampling artifacts in the Los Angeles Basin. *Atmos. Environ.* **1994**, *28*, 3061−3071, Research & Development.
(25) Turn, S. Q.; Jenkins, B. M.; Chow, J. C.; Pritchett, L. C.; Campbell, D. E.; Cahill, T. A.; Whalen, S. A. Elemental characterization of particulate matter emitted from biomass burning: Wind tunnel derived source profiles for herbaceous and wood fuels. *J. Geophys. Res.* **1997**, *102*, 3683−3699.
(26) Chen, L.-W. A.; Chow, J. C.; Watson, J. G.; Moosmüller, H.; Arnott, W. P. Modeling reflectance and transmittance of quartz-fiber filter samples containing elemental carbon particles: Implications for thermal/optical analysis. *J. Aerosol Sci.* **2004**, *35*, 765−780, doi: 10.1016/j.jaerosci.2003.12.005.
(27) Cao, J. J.; Wu, F.; Chow, J. C.; Lee, S. C.; Li, Y.; Chen, S. W.; An, Z. S.; Fung, K. K.; Watson, J. G.; Zhu, C. S.; Liu, S. X. Characterization and source apportionment of atmospheric organic and elemental carbon during fall and winter of 2003 in Xi'an, China. *Atmos. Chem. Phys.* **2005**, *5*, 3127−3137, 1680−7324/acp/2005-5-3127.
(28) Kim, E.; Hopke, P. K. Source apportionment of fine particles at Washington, DC, utilizing temperature-resolved carbon fractions. *J. Air Waste Manage. Assoc.* **2004**, *54*, 773−785.
(29) Chen, L.-W. A.; Chow, J. C.; Watson, J. G.; Magliano, K. Quantifying $PM_{2.5}$ source contributions for the San Joaquin Valley with multivariate receptor models. *Environ. Sci. Technol.* **2007**, *41* (8), 2818−2826.
(30) Watson, J. G.; Chow, J. C.; Lowenthal, D. H.; Pritchett, L. C.; Frazier, C. A.; Neuroth, G. R.; Robbins, R. Differences in the carbon composition of source profiles for diesel- and gasoline-powered vehicles. *Atmos. Environ.* **1994**, *28*, 2493−2505.
(31) Chow, J. C.; Watson, J. G.; Kuhns, H. D.; Etyemezian, V.; Lowenthal, D. H.; Crow, D. J.; Kohl, S. D.; Engelbrecht, J. P.; Green, M. C. Source profiles for industrial, mobile, and area sources in the Big Bend Regional Aerosol Visibility and Observational (BRAVO) Study. *Chemosphere* **2004**, *54*, 185−208.
(32) Chen, L.-W. A.; Doddridge, B. G.; Dickerson, R. R.; Chow, J. C.; Mueller, P. K.; Quinn, J.; Butler, W. A. Seasonal variations in elemental carbon aerosol, carbon monoxide, and sulfur dioxide: Implications for sources. *Geophys. Res. Lett.* **2001**, *28*, 1711−1714.
(33) Dickerson, R. R.; Andreae, M. O.; Campos, T.; Mayol-Bracero, O. L.; Neusuess, C.; Streets, D. G. Analysis of black carbon and carbon monoxide observed over the Indian Ocean: Implications for emissions and photochemistry. *J. Geophys. Res.* **2002**, *107*, 8017, doi: 10.1029/2001JD000501.

Received for review October 4, 2006. Revised manuscript received February 23, 2007. Accepted March 22, 2007.

ES062364I